Star Formation in Space and Time: The Orion Nebula Cluster

E. M. Huff and Steven W. Stahler

Astronomy Department, University of California, Berkeley, CA 94270

ABSTRACT

We examine the pattern of star birth in the Orion Nebula Cluster (ONC), with the goal of discerning the cluster's formation mechanism. Outside of the Trapezium, the distribution of stellar masses is remarkably uniform, and is not accurately described by the field-star initial mass function. The deconvolved, three-dimensional density of cluster members peaks at the Trapezium stars, which are truly anomalous in mass. Using theoretical pre-main-sequence tracks, we confirm the earlier finding that star formation has accelerated over the past 10^7 yr. We further show that the rate of acceleration has been the same for all masses. Thus, there is no correlation between stellar age and mass, contrary to previous claims. Finally, the acceleration has been spatially uniform throughout the cluster.

Our reconstruction of the parent molecular cloud spawning the cluster shows that it had a mass of 6700 $M_\odot$ prior to its destruction by the Trapezium. If the cloud was supported against self-gravity by mildly dissipative turbulence, then it contracted in a quasi-static, but accelerating manner. We demonstrate this contraction theoretically through a simple energy argument. The mean turbulent speed increased to its recent value, which is reflected in the present-day stellar velocity dispersion.

The current ONC will be gravitationally unbound once cloud destruction is complete, and is destined to become a dispersing OB association. We hypothesize that similarly crowded groups seen at the centers of distant OB associations are also unbound, and do not give rise to the Galactic population of open clusters. Finally, accelerating star formation implies that most clumps within giant molecular complexes should have relatively low formation activity. Sensitive infrared surveys could confirm this hypothesis.

Subject headings: stars: formation — stars: pre-main sequence — open clusters and associations: individual (Orion Nebula Cluster)

1. Introduction

The origin of stellar groups is one of the abiding mysteries of astronomy. Infrared and radio observations have demonstrated that these aggregates are born within cold molecular clouds (Lada & Lada 2003). We also know that young groups come in three varieties – T associations, open clusters, and OB associations. Yet we have little notion as to what distinguishes the progenitor cloud for each type.

The statistics of stellar births on the Galactic scale indicates that most stars originate in OB associations (Roberts 1957; Miller & Scalo 1978). These populous groups form inside clumps within giant molecular complexes (Blitz 1993). The parent clump must have attained a high density at the formation site of the massive O and B stars, since the youngest of these are almost always found in crowded stellar fields (e.g., Stahler *et al.* 2000). But how did the cloud attain such a high density? More generally, what forces drove its evolution as it was producing the association?

By far the best-studied young OB association is the Orion Nebula Cluster. Over a thousand members are seen only in the near-infrared (Ali & Depoy 1995). However, a comparable number are optically visible (*e.g.*, Prosser *et al.* 1994), since much of the parent cloud is now dispersed. Foreground neutral gas is largely confined to a relatively thin layer (O'Dell *et al.* 1992), while gas ionized by θ^1 Ori C and its massive companions is being driven outward (Gordon & Churchwell 1970; O'Dell 1994). Behind this hemispherical blister of stars and ionized gas lies a dense, massive wall of molecular gas, still creating new stars (see, *e.g.*, Genzel & Stutzki 1989).

In this paper, we examine anew both the present morphology of the cluster and its past record of star formation. Our goal is to elucidate, as much as possible, the properties and dynamical history of the parent cloud body. This contribution is the latest in a continuing investigation of stellar groups and their origin. Palla & Stahler (1999; hereafter Paper I) found that star formation in this region has been accelerating over time, a result seen generally, albeit at a reduced level, in other nearby groups (Palla & Stahler 2000; Paper II). In a study of pre-main-sequence binaries, Palla & Stahler (2001) showed that the companion to BM Ori is no older than 10^5 yr. It thus apears that the centrally located Trapezium stars were formed relatively recently. Here, we wish to provide a fuller account of the region's evolution in both space and time, and to draw implications for stellar group formation generally.

Our main results may be readily summarized. The Trapezium stars are truly anomalous within the group, with a total mass equivalent to hundreds of ordinary stars. Excluding the Trapezium, the distribution of stellar masses is nearly uniform throughout the remaining

cluster. The fractional increase with time in the stellar population has also been the same at all locations. In other words, the acceleration in starbirth, which occurred over some 10^7 yr, was a *global* phenonemon, and resulted in a remarkably homogeneous membership, except at the very center.

We hypothesize that this rise in star formation activity was stimulated by large-scale contraction of the ONC parent cloud. The gas density must have increased in a quasi-static, but accelerating manner. We explore a simple model, in which the cloud was supported against self-gravity by turbulent pressure. The energy associated with this turbulent motion is continually dissipated by internal shocks. In our model, the mean turbulent speed *increases* with time because of gravitational compression. Energy dissipation from shocks also increases, which allows faster contraction. In summary, our model illustrates how accelerating contraction, along with a concurrent rise in star formation, is a natural and generic consequence of support from internal turbulence.

Section 2 below presents our analysis of the present-day ONC stellar distribution. In Section 3, we utilize pre-main-sequence stellar ages to infer the star formation history throughout the region. Section 4 offers our physical interpretation of this history in terms of the parent cloud and its evolution. Finally (§5), we discuss the implications of this study, both for the ONC and for stellar group formation generally.

2. Current Stellar Population

2.1. Density Variation

Our empirical dataset comes from the important study by Hillenbrand (1997). Combining her own observations with the existing literature, Hillenbrand obtained both optical spectra and V- and I-band fluxes for 934 stars within 2.5 pc of the Trapezium. A comparable number of stars are detectable only at near-infrared wavelengths (Ali & Depoy 1995). The optical spectra yielded spectral types, which in turn gave effective temperatures. Observed V-I colors were then employed to find individual extinctions. A bolometric correction to the I-magnitudes, together with the extinction, then gave stellar luminosities. In this manner, the stars were placed in the theoretical HR diagram, *i.e.*, the L_*-$T_{\rm eff}$ plane.

Figure 1 shows the positions of a large subsample, 705 stars, from the full, optically visible set. These are the objects that, according to Hillenbrand, have a membership probability exceeding 67 percent. These probabilities were assessed from earlier proper-motion studies, principally that of Jones & Walker (1988). As is well known, the stars are crowded toward θ^1 Ori C, whose own position is central in the plot. The conspicuous gap in stars just

to the east of the Trapezium coincides with the Dark Bay, familiar from optical photographs of the region (*e.g.*, Pogge et al. 1992).

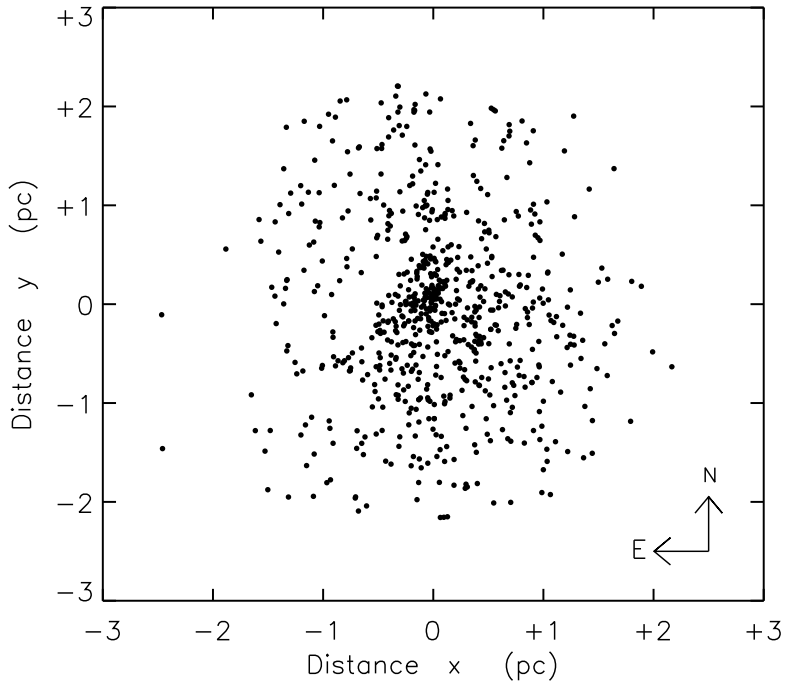

Fig. 1.— Positions in the sky of the 705 ONC stars with 67 percent membership probability (from Hillenbrand 1997). The x- and y-axis are oriented in the directions of right ascension and declination, respectively, and a distance of 480 pc is assumed.

What is the true, three-dimensional distribution of these stars? It has long been accepted that the visible population is contained within an ionized blister of gas, located in front of OMC-1, itself a portion of the extended Orion A cloud (Zuckerman 1973). Wen & O'Dell (1995) used the distribution in Hα emission to map out the ionized front surface of OMC-1. They found that the main ionizing source, θ^1 Ori C, is situated only 0.2 pc from this rear wall. (See their Figure 3.) This distance is small compared to the full cluster diameter of 5 pc. Hence we may assume, with little loss of precision, that the ONC morphology is hemispherical.[1]

[1]The full cluster morphology may be spherical. If so, the many near-infrared sources imaged by Ali & Depoy (1995) and by Hillenband & Carpenter (2000) plausibly represent the rear half of the sphere, *i.e.*, that fraction partially embedded in the OMC-1 wall.

Working within this model, we first azimuthally average the projected stellar distribution, again choosing θ^1 Ori C as our origin. In Figure 2 we show this empirical distribution as a function of the radius r. The quantity displayed is the number of stars enclosed at each r-value. This cumulative number is then converted to a fraction of the total stellar population, and denoted as $f_*(r)$.

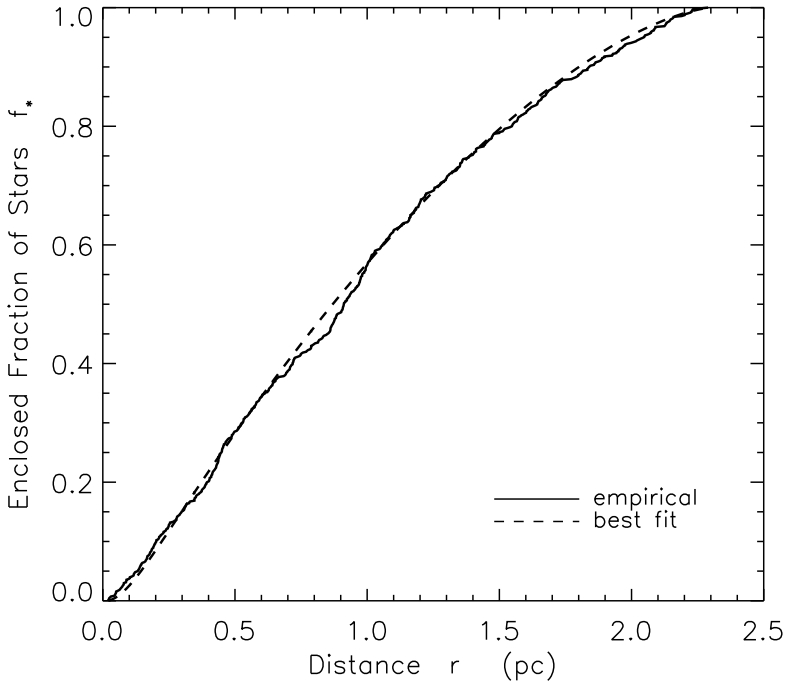

Fig. 2.— The projected number density of stars. The fraction of the total stellar population of 705 stars is shown as a function of projected radius. The dashed curve is a smooth fit to the data.

We fit these data by adopting a simple form for the three-dimensional stellar number density throughout the hemisphere:

$$n_*(r) \;=\; n_c \left[1 \;-\; \frac{r}{r_1} \;+\; \left(\frac{r}{r_2}\right)^2\right]^{-1} \quad . \tag{1}$$

For each choice of the scale lengths r_1 and r_2, we project this density onto the plane of the sky and compute the cumulative number fraction $f_*(r)$. We then vary r_1 and r_2 until our model $f_*(r)$ best matches the empirical curve. Note the negative sign preceding the term containing r_1; this choice is necessary to match the relatively rapid rise in the observed $f_*(r)$

away from the origin. Note also that the central density n_c is unconstrained by this matching procedure.

The smooth curve in Figure 2 shows the best-fit $f_*(r)$, obtained by selecting $r_1 = 0.25$ pc and $r_2 = 0.14$ pc. To estimate the central density, we integrate equation (1) over the entire hemisphere and equate the total number of stars to the observed 705. We thus find $n_c = 2300$ pc^{-3}. This result is close to that given by Herbig & Terndrup (1986), who surveyed the inner 0.5 pc in radius. Both numbers are dwarfed by the density of 5×10^4 pc^{-3} found in the high-resolution, near-infrared study of McCaughrean & Stauffer (1994). Their high value was obtained by counting stars within 0.05 pc of θ^1 Ori C, a distance comparable to that of the other Trapezium members.

It is interesting that the stellar number density falls off as r^{-2} for $r \gg r_2$. Of course, we forced this result mathematically through our adopted functional form of $n_*(r)$. We were guided in this choice by previous authors, who noted that the *projected* areal density falls approximately as r^{-1} (see, *e.g.*, Scally & Clarke 2001). How robust is this result? We have generalized equation (1) to include an exponent $2+\epsilon$ in the term involving r_2. We then varied ϵ along with r_1 and r_2 in our matching procedure. An acceptable fit, in the least-squares sense, could only be obtained for ϵ ranging from -0.1 to +0.4.

If this r^{-2} falloff continued to very large radii, the cumulative, projected starcount would increase as r. According to Figure 2, the rise is actually slower, both observationally and in the theoretical fit. We are seeing the effect of a finite boundary, corresponding to 2.5 pc in radius. Outside this boundary, no stars are counted.[2] Of course, the stellar population does not truly vanish, but there is a steeper falloff in this vicinity, as the central group blends into the larger Orion Ic association (Herbig & Terndrup 1986).

Figure 3 displays the reconstructed, three-dimensional density $n_*(r)$. One notable feature here is the central dip. However, the results of McCaughrean & Stauffer (1994) indicate that this falloff, which occurs for $r \lesssim 0.05$ pc, is not real. The true stellar density climbs steeply toward the center. At visible wavelengths, this interior population is lost in the brilliant glare of the Trapezium. It is at least partially recovered in high-resolution, near-infrared imaging. (See also Hillenbrand & Carpenter 2000.) The dashed curve in Figure 3 is a pure r^{-2} profile. Extended inward, its rise is suggestive of that found empirically within 0.05 pc.

---

[2]A singular isothermal sphere truncated at radius R has a projected surface density which varies as r^{-1} times the correction factor $\arctan\sqrt{(R/r)^2 - 1}$.

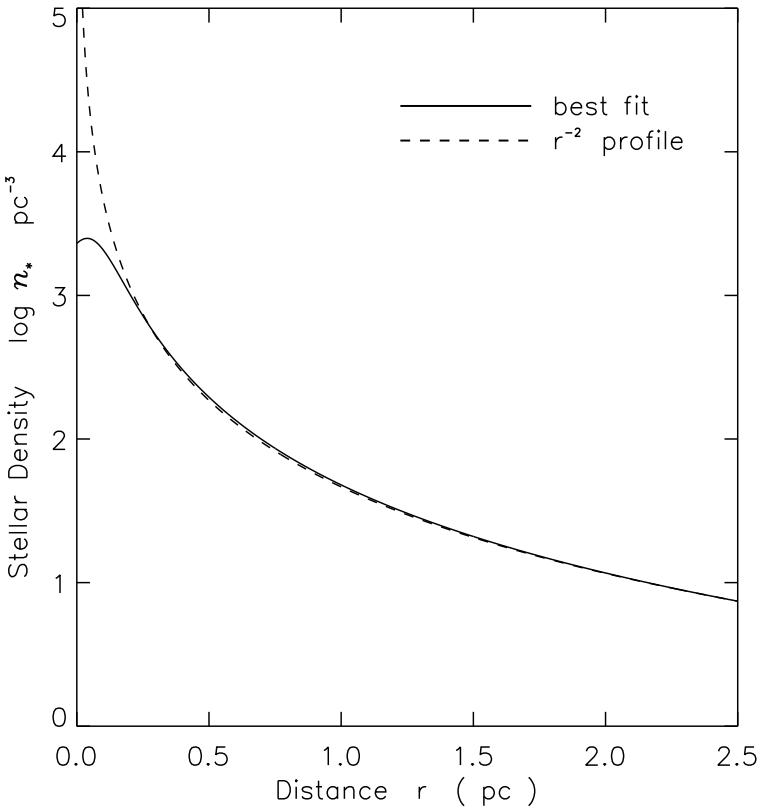

Fig. 3.— Reconstructed, three-dimensional density of stars, compared to a r^{-2} profile (*dashed curve*). The inward falloff in the reconstructed density is not real, but reflects incompleteness of the optical sample in the crowded central region.

2.2. Mass Distribution

We turn next to the spatial distribution of stellar masses in the present-day cluster. To obtain a full sampling of masses among the optical population, we need to consider the sensitivity limit of the original survey. Here we are concerned with spectroscopic observations, which are needed to place stars in the HR diagram.

According to Hillenbrand (1997), her observations are complete to $I = 17$. (See upper panel of her Figure 6.) A typical ONC star is of spectral type M2, for which $V - I = 2.4$. The bolometric correction needed to extrapolate from the V-band to $M_{\rm bol}$ is -1.8 mag (Hillenbrand 1997; Appendix C). For the representative extinction $A_V = 2$, and the distance modulus of 8.4 mag, we find that the limiting I-magnitude corresponds to a luminosity of 0.1 $L_\odot$.

We may now address the completeness of stellar masses. Suppose we limit our investigation to stars with ages less than 1×10^7 yr. Then the lowest stellar mass for which we have complete data is that whose pre-main-sequence track descends to 0.1 $L_\odot$ at $t = 1 \times 10^7$ yr. Inspection of Figure 1 from Palla & Stahler (1999) shows that this critical mass is 0.4 $M_\odot$. When discussing stellar masses and ages, we will henceforth limit our attention to the restricted sample of 244 stars with $M_* \geq 0.4\ M_\odot$.

It is important to note that the failure to account for survey completeness may lead to puzzling and erroneous results. For example, Hillenbrand (1997) observed that lower-mass stars in both Orion and other regions are younger, on average, than their high-mass counterparts. This age discrepancy was noted again by Hartmann (2004), and led him to reject the pre-main-sequence tracks themselves as reliable age indicators. However, the lower-mass population is incompletely sampled in all surveys. The missing objects are precisely those of lower luminosity, and hence greater ages. Within our more carefully defined sample, we find no age-mass correlation (see §3 below).

We now wish to explore both the distribution of masses and how this distribution varies spatially in the cluster. A simple but instructive exercise is to divide the cluster into two groups of equal population. The inner group lies within a circle of radius 0.88 pc, centered on θ^1 Ori C. The outer group is in the surrounding annulus. We rank stars in each group by mass, and calculate the fraction of the group at or below every mass-value. To construct the figure, we find, for each mass in one group, that mass in the other group which represents the same cumulative fraction. (Such a *quantile-quantile plot* is a common statistical tool for comparing populations; see Evans et al. 2000).

Figure 4 shows the result. The vast majority of stars match up, *i.e.*, the two populations are essentially identical. (The step-like character of the empirical curve is an artifact of the discrete spectral typing.) Above $M_* \approx 3\ M_\odot$, however, the two populations differ radically. The inner group contains objects which are more massive than any found outside. Naturally, the Trapezium stars are part of this exceptional subgroup. Figure 4, which displays masses on a logarithmic scale, shows vividly how the Trapezium is truly anomalous. If we ignore its central region, the cluster appears to be homogeneous in terms of membership.

Another way to demonstrate this point is presented in Figure 5. The dashed curve in both panels represents the cumulative mass fraction, *i.e.*, the fraction of the total cluster mass contained in each radius r. The solid curve is the cumulative number fraction. If we include the Trapezium (*left panel*), the mass fraction immediately rises above the number fraction. If we omit the Trapezium (*right panel*), the mass and number fractions are nearly identical from the center outward. In other words, increasing the number of stars by a certain fraction gives the same fractional increase in mass, at all radii. The distribution of individual

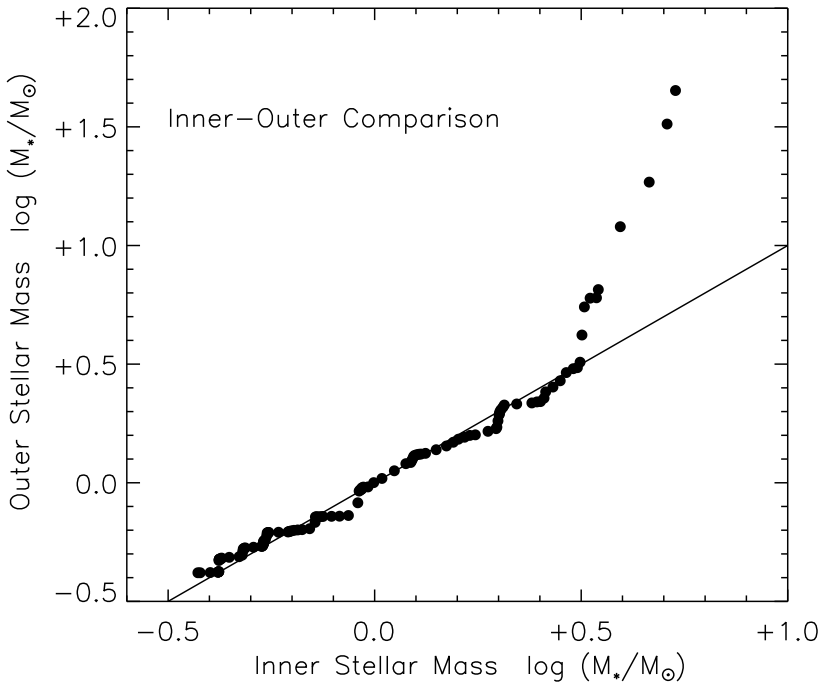

Fig. 4.— Comparison of stellar masses in the inner and outer halves of the cluster. Note the anomalously massive stars within the inner region.

stellar masses must therefore be similar throughout the cluster. Clearly, we are not seeing mass segregation in the traditional sense.

It also follows that the local mass distribution is essentially the same as the global one. Paper I (§4) asserted that the ONC stars roughly follow the field star initial mass function. The top two curves of Figure 6 show that the two distributions actually differ in a significant way. The solid curve displays the cumulative mass function $\mathcal{N}_*(M_*)$, *i.e.*, the number of stars with masses up to the value M_*. For comparison, the dashed curve shows the same quantity calculated from the field star initial mass function (Scalo 1998). (This and the other dashed curves are normalized to the total population in each age range). It is apparent that the ONC is deficient in members with $0.8\ M_\odot \lesssim M_* \lesssim 3.0\ M_\odot$. A similar discrepancy appears in the analysis of Hillenbrand (1997), although she used different pre-main-sequence tracks and a different field-star initial mass function. (See the upper panel of her Figure 15.) The remaining curves of Figure 6 concern the temporal development of the cluster, and it is this subject that we now consider.

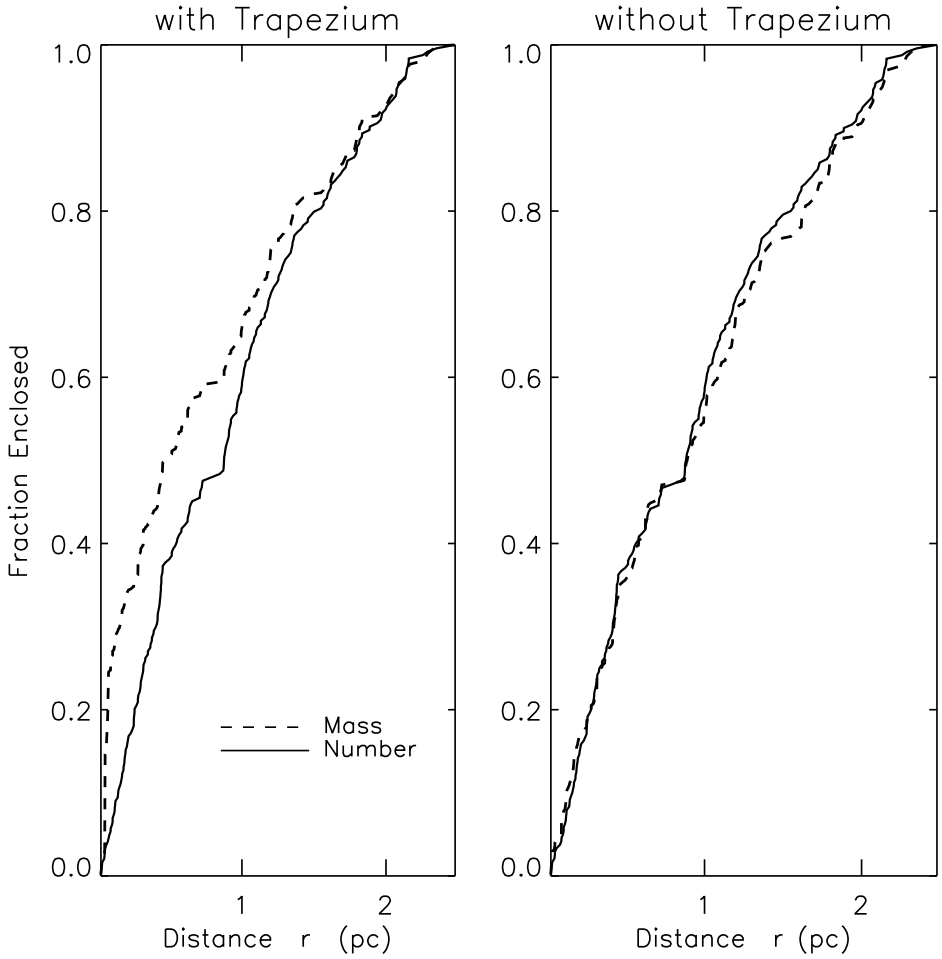

Fig. 5.— Comparison of the distributions of stellar mass and number as a function of radius. *Left panel:* When the Trapezium is included, the mass curve immediately climbs higher than the stellar number. *Right panel:* Without the Trapezium, the two distributions are nearly identical, indicating uniformity of the stellar mass spectrum.

3. Star Formation History

The distribution of pre-main-sequence ages provides the essential record of star formation in any group. Palla & Stahler (1999) used this technique to show that production of stars within the ONC began some 10^7 yr in the past and has been accelerating to the present. We now go one step further, and combine stellar ages and *locations*. In other words, we assess the evolution of the region both temporally and spatially.

The four panels of Figure 7 display maps of the ONC at various epochs. Within each

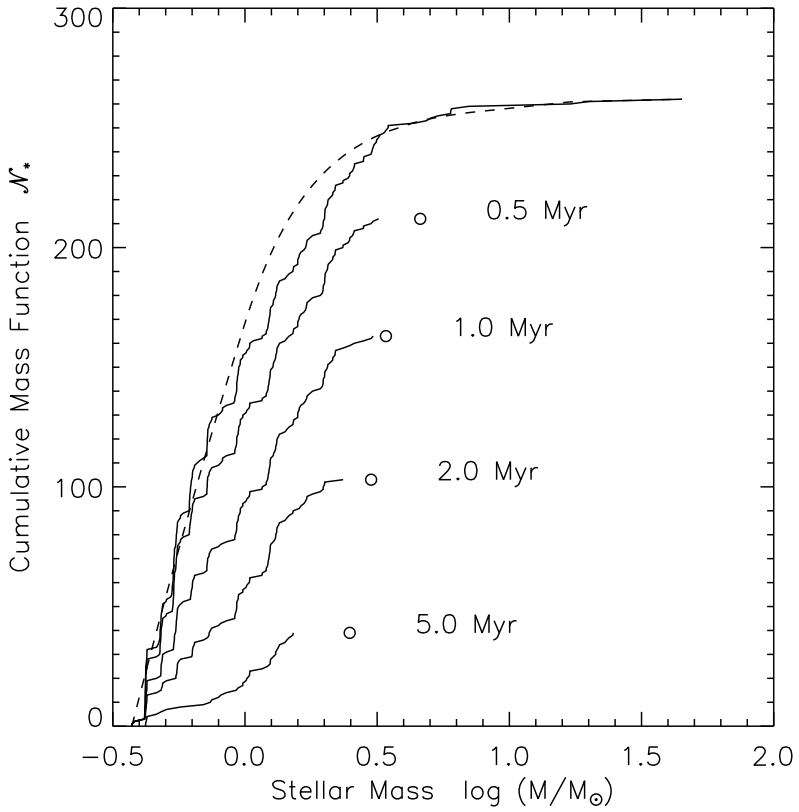

Fig. 6.— The cumulative mass function for stars of different ages. The bottom curve represents only stars older than 5 Myr; the next curve is for stars older than 2 Myr, etc. The top curve shows this function for the entire sample of 244 stars. Each open circle marks the stellar mass whose pre-main-sequence lifetime is the value indicated. The dashed curve was constructed from the field-star initial mass function of Scalo (2002).

time interval (given in the caption), the panel shows all stars from the sample of 244 that were born during that interval. The small symbols denote low-mass objects ($M_* < 2\ M_\odot$), while the larger ones represent those of intermediate mass ($2\ M_\odot < M_* < 8\ M_\odot$). We have omitted the three innermost Trapezium stars, which would not be resolved in these plots. None of these three have reliable ages, although they were probably formed within the most recent epoch (Palla & Stahler 2001). Note that the lowest-mass Trapezium star, BM Ori, has 7 $M_\odot$, and is thus included in the final map.

It is apparent that the earliest star formation, which occurred some 10^7 yr in the past, was diffuse spatially, and did not exhibit crowding toward the future site of the Trapezium. Intermediate-mass stars also began forming early, and were also spread throughout the re-

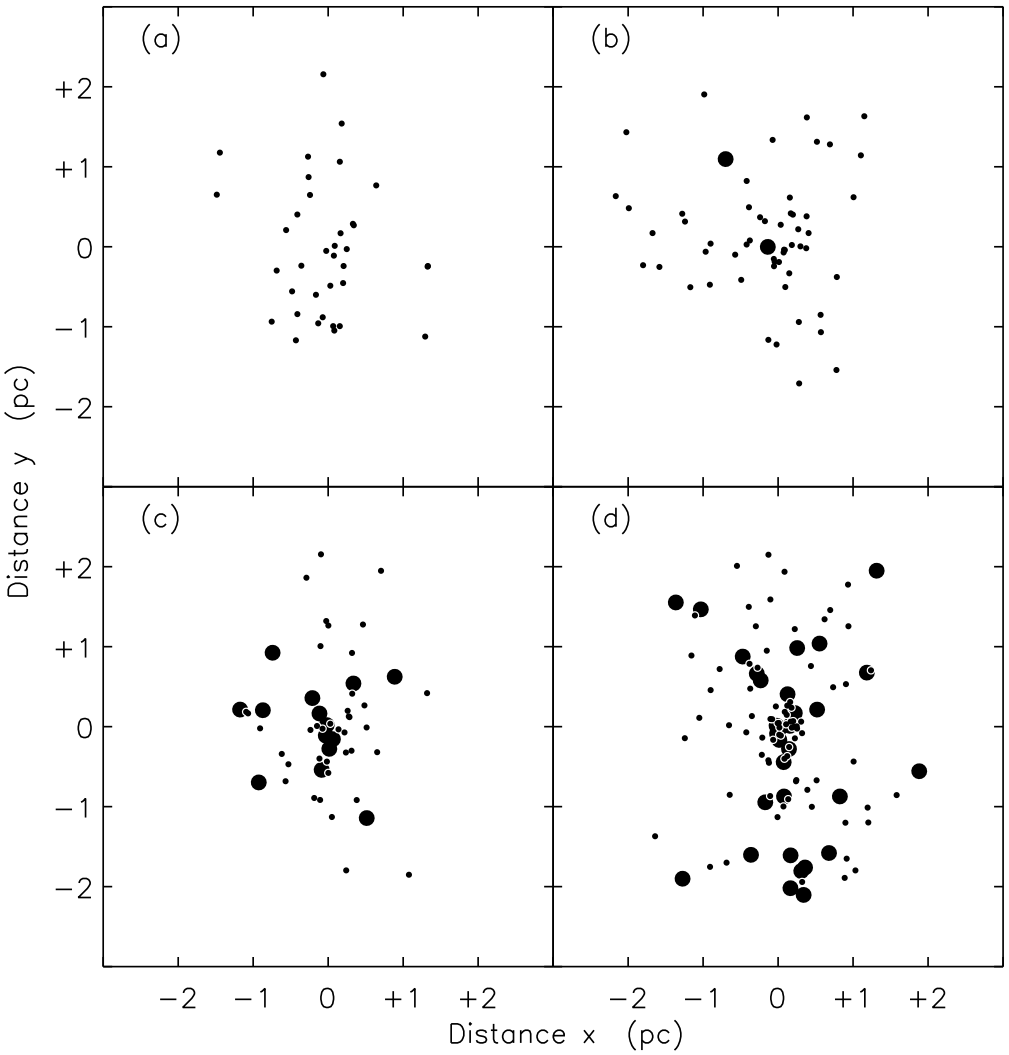

Fig. 7.— Positions of ONC stars (from the sample of 244) that were born (a) more than 5 Myr ago, (b) from 2 to 5 My ago, (c) from 1 to 2 Myr ago, and (d) more recently than 1 Myr. The smaller filled circles denote stars with $M_* < 2\,M_\odot$, while the larger ones are for $2\ M_\odot < M_* < 8\ M_\odot$

gion. As expected, the entire population increased dramatically within the last few Myr. No star formation is occurring now within the volume occupied by the visible stars, since molecular gas has been driven off. If, however, the cluster extends into the wall of OMC-1, then starbirth is undoubtedly continuing apace in that embedded region.

The ONC stars have transverse velocities of several km s^{-1} (Jones & Walker 1988). Over

10^7 yr, they would have moved tens of parsecs, well out of the area shown. How, then, can we identify their present positions with their birth sites? The reason is that *the stars have not been moving on ballistic trajectories*. They have been subject to the gravitational pull from other cluster members and, much more significantly, from the ambient molecular gas. In other words, they were trapped in local potential wells until recently, when the nearby gas was ionized and dispersed. If this dispersal occurred 10^5 yr ago, then the stars subsequently moved only a few tenths of a parsec.

We also arrive at this picture of the stellar motion by following the consequences of the alternative view. Suppose that all stars were born in the most crowded region, near the present-day Trapezium. Suppose further that they drifted away from their birth sites at constant speed. Then we would see today an age gradient, in the sense that the older stars would be farther from the center. Figure 8 plots the mean stellar age at each projected radius, along with the rms dispersion. The mean age does not increase outward, but remains constant to within the statistical errors. Under the drift hypothesis, furthermore, proper motion vectors would tend to point outward for more distant members. This effect is also not seen; the vectors are randomly oriented (Jones & Walker 1988).

A plot of the mean age versus stellar mass is also of interest, especially in light of the previous claims for a correlation (Hillenbrand 1997; Hartmann 2004). Figure 9 shows the result. When we limit ourselves to the sample of 244 stars, the mean pre-main-sequence age is essentially independent of mass, at least for $M_* \lesssim 2.5\ M_\odot$. For higher masses, the mean age does systematically fall, in apparent agreement with the earlier claims.

However, this falloff only reflects the diminishing pre-main-sequence lifetime of more massive objects. The dashed curve displays this lifetime, *i.e.*, the contraction time from the birthline to the zero-age main sequence, as a function of mass. Above 2.5 $M_\odot$, a significant fraction of the stars have already reached the main sequence. However, all stars in the sample are assigned *pre*-main-sequence ages, according to their positions on the HR diagram. The main-sequence stars thus have ages which are too young. Since the relevant fraction increases with stellar mass, there is a spurious correlation of age with mass.

Returning to the global evolution, the sequential maps of Figure 7 demonstrate that star formation is accelerating, but they do not tell us the spatial pattern of that acceleration. Is the increase of stellar births predominantly near the center? Has the acceleration process perhaps moved inward over time? Such details are important if we are to discern the physical processes at play in group formation.

It is again instructive to divide the cluster into two groups of equal population, as we did when constructing Figure 4. This time, we compare the star formation histories of the

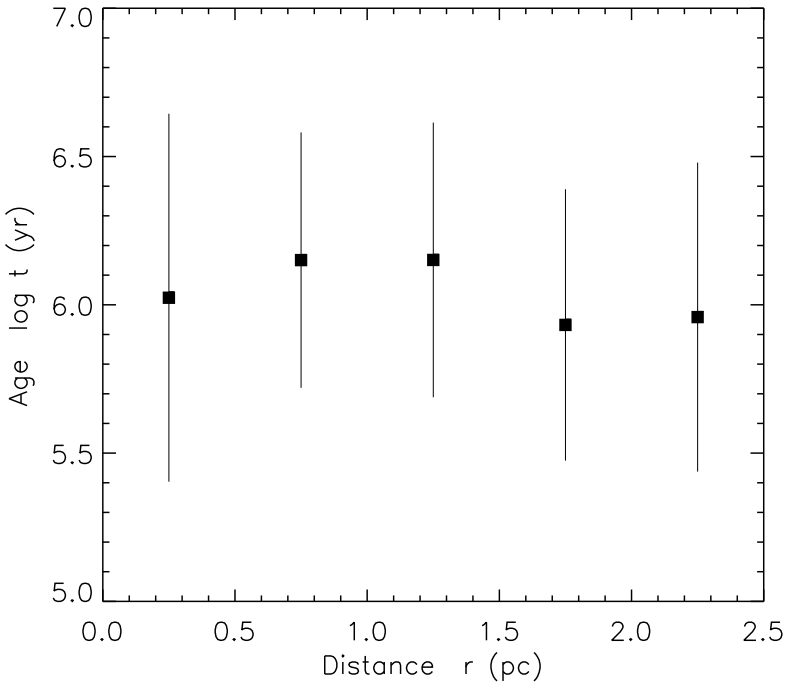

Fig. 8.— Pre-main-sequence stellar age as a function of projected radius. Shown is $\log t$, averaged within an annulus centered on each displayed radius. The rms error is also shown at each position.

inner and outer portions of the cluster. The result is shown in Figure 10. Here we display the fraction of stars in each group that have at least the indicated ages. In other words, we are showing that portion of each group formed at any time. The two curves are nearly identical.

What we have found is that the acceleration did not occur locally. Nor did it sweep across the parent cloud. In fact, there is no known mechanism by which low-mass star formation in one region can stimulate formation in another, distant region. The accelerating star formation occurred globally. This process must have been stimulated by contraction of the parent cloud.

We mentioned previously that the present-day distribution of masses differs somewhat from the canonical initial mass function. Returning to Figure 6, we find that this distribution changed substantially as time progressed. Here, the series of lower curves shows the cumulative mass function $\mathcal{N}_*$ at the indicated times. Thus, the bottom curve represents the number of stars with mass less than any M_* which are older than 5 Myr. Relatively few

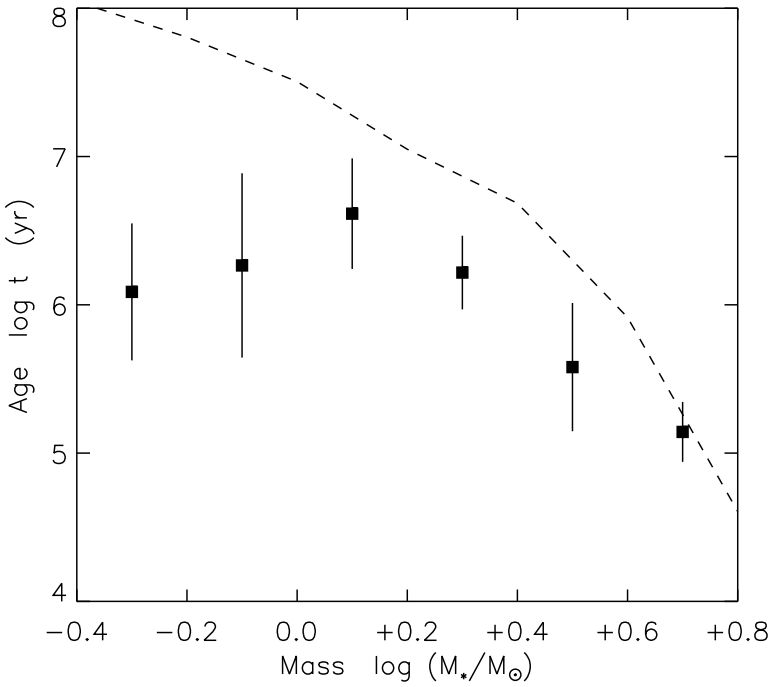

Fig. 9.— Pre-main-sequence stellar age as a function of mass. This plot was constructed in a manner analogous to Figure 8. The dashed curve represents the total contraction time to the zero-age main sequence at each mass value.

stars have the requisite age. The figure shows, not surprisingly, that their mass spectrum also does not resemble the standard initial mass function.

What determines the upper mass cutoff at each epoch? It is tempting to hypothesize that no relatively massive stars existed long ago because there had not yet been sufficient time to form them. However, the figure itself suggests an alternative explanation. The open circles show the masses for which the pre-main-sequence lifetime equals the age in question. (Compare the dashed curve of Figure 9.) At all times, the maximum mass is fairly close to this limit. In other words, more massive stars could have indeed formed, but they already would have joined the main sequence. If such objects were (erroneously) assigned contraction ages, the latter would necessarily be less than the corresponding time.

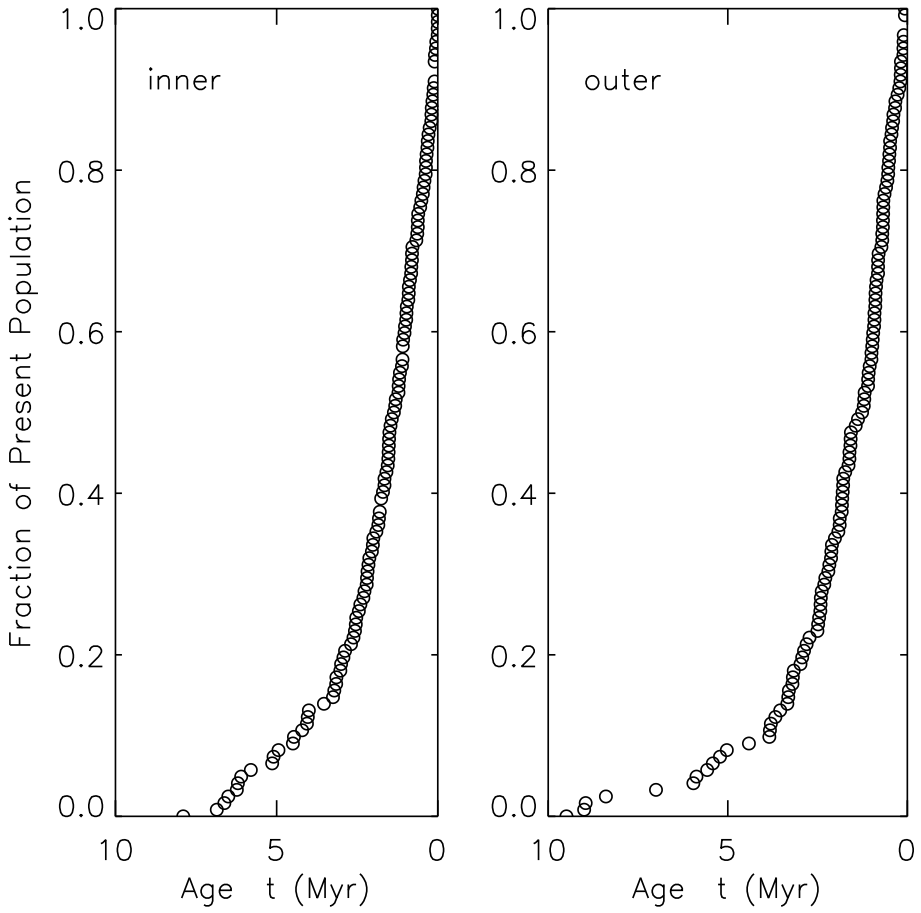

Fig. 10.— Acceleration of starbirth in the inner and outer regions of the cluster. Plotted in each panel is the fraction of the present population that has the indicated age.

4. Physical Interpretation

4.1. Cloud Mass

We have seen how the present number density of stars, $n_*(r)$, peaks at a very high central value. Since the parent cloud was only recently dispersed, its own density must have similarly peaked. The gas itself was not smoothly distributed, but consisted of clumps, many of which already contained the stars we see today. Averaging over such clumps, what might have been the radial falloff in density and the total cloud mass, just prior to dispersal?

A second clue comes from the observed proper motions of stars. Jones & Walker (1988)

found the vectors to be randomly oriented in the sky; the component in any direction has a mean magnitude of 2.4 km s^{-1}. The spread in proper motion magnitudes is relatively small, about 0.2 km s^{-1}.[3] If the stars were indeed trapped in the gas before dispersal, then we may interpret their speed as the one-dimensional velocity of the cloud gas. The observed randomness in orientation of the stellar velocities implies that the corresponding gas motion was similarly random. That is, the internal bulk motion of the cloud was turbulent. We equate the stellar proper velocity in any direction with $V_{\rm turb}$, the one-dimensional turbulent speed.

It is conventional to model the momentum transfer associated with such turbulent motion as arising from the pressure of an ideal gas. Then our cloud is effectively a self-gravitating, isothermal sphere. Because of the central peak, it is specifically the singular isothermal sphere, with a density given by

$$\rho(r) \, = \, \frac{V_{\rm turb}^2}{2\,\pi\,G\,r^2} \ , \tag{2}$$

and a total mass of

$$M_{\rm cloud} \, = \, \frac{2\,V_{\rm turb}^2\,R}{G} \tag{3}$$

inside the radius R. For a cluster radius of 2.5 pc and the $V_{\rm turb}$-value taken from the stellar data, we find that $M_{\rm cloud} \, = \, 6700 \ M_\odot$. Note that we have taken the cloud to be a full sphere, whose foreground half produced the visible stars. For comparison, the total mass of these stars is only 480 $M_\odot$ for the sample of 244, and 580 $M_\odot$ for the larger group of 705.[4]

4.2. Turbulent Dissipation

Our estimate of the ONC cloud mass rests on the assumption that self-gravity balanced turbulent pressure just prior to dispersal. How well is this assumption supported by observation? It has long been known that the line widths of optically thin tracers yield fluid velocities consistent with virial values, over a large range of masses and sizes (Larson 1981; Myers & Goodman 1988). This finding is generally interpreted to mean that clouds are indeed supported by internal, turbulent motion.

---

[3]There is a potential problem in calculating this dispersion for a sample of stars chosen by a membership criterion based on the proper motions themselves. However, Jones & Walker (1988) noted that the calculated dispersion is insensitive to the precise membership criterion.

[4]Hillenbrand (1997) claims that her sample extends below a true turnover in the luminosity function. Hence, our total mass estimate for the visible stars should be reasonably accurate.

Motivated by the observations of superthermal linewidths, a number of theorists have modeled, through direct numerical simulation, the dynamics of turbulence in a magnetized cloud gas. (See Vázquez-Semadeni *et al.* 2000 for a review of such calculations.) Although the simulations adopted a variety of assumptions concerning the impressed turbulence, the results have been qualitatively consistent. In the absence of persistent driving, the turbulence decays rapidly, typically within a few crossing times. This time is set by the average eddy speed and the size of the computational box. Mac Low (1999) has determined the energy dissipation rate from a suite of MHD simulations. His essential conclusion is

$$\dot{\epsilon} \, = \, -\eta \, \frac{V_{\rm turb}^3}{\lambda} \ . \tag{4}$$

Here, $\dot{\epsilon}$ is the energy loss rate per unit mass of gas, $V_{\rm turb}$ the average (rms) eddy speed, and λ the dominant wavelength of the impressed turbulence. The empirical, nondimensional coefficient η was found to be about 0.4 in these simulations.

These important experiments are actually finding *two* results; both may not be applicable to real molecular clouds. The first, and more basic, finding is that MHD turbulence is dissipative. Even incompressible modes (Alfvén waves) quickly transfer energy to compressive waves, which steepen and shock (Goldstein 1978; see also the discussion in Stone et al. 1998). This result is physically compelling, even if the actual dissipation in the simulations is numerical in origin.

The second result, more problematic astrophysically, is that the turbulence quickly decays. Here we must bear in mind that all the simulations are local. Any global compression of the cloud due to self-gravity cannot be modeled. But that very compression should supply energy and help sustain the turbulence. Indeed, if the mean eddy speed is to match the virial value at all times, as observations suggest, then that speed should *increase with time.* Furthermore, if the cloud contraction is mediated by turbulent dissipation, then this contraction naturally accelerates.

4.3. Accelerating Contraction

Let us illustrate these considerations through a simple, heuristic model, inspired by our reconstruction of the ONC cloud. The total energy, gravitational plus thermal, of the cloud in the recent past is that of the bounded, singular isothermal sphere. For a cloud of mass $M_{\rm cloud}$ and radius R, this energy is given by

$$E \, = \, -\frac{1}{4} \, \frac{G \, M_{\rm cloud}^2}{R} \ . \tag{5}$$

What was the cloud structure at previous times? The strong central peak in density was presumably attained just prior to the formation of the Trapezium, *i.e.*, within the last 10^5 yr. It is reasonable to assume that the cloud's density contrast monotonically increased with time to that point. If the turbulent velocity was also spatially homogeneous during earlier epochs, then the cloud evolved through a sequence of isothermal spheres, culminating in the singular configuration.

The evolution is driven by self-gravity, mediated by the energy loss from turbulence. This bulk motion continually drives internal shocks, which themselves radiate energy at a *local* rate given by equation (4). If the largest eddy has a size λ comparable to the cloud diameter, then the mass-integrated heat equation is

$$\frac{dH}{dt} \;=\; -\eta\,\frac{M_{\rm cloud}\,V_{\rm turb}^3}{2\,R}\;. \tag{6}$$

The quantity H is the cloud enthalpy, equal to $E_{\rm tot} + P_\circ\,V$. Here, $P_\circ$ is the bounding pressure, and V the cloud volume. As we show in the Appendix, it is this quantity whose decrease yields the cloud's total, shock-generated luminosity. We regard η as a free parameter, whose value we expect to be less than that found in the current local simulations.

For the singular isothermal sphere, the enthalpy is

$$H \;=\; -\frac{1}{12}\,\frac{G\,M_{\rm cloud}^2}{R}\;. \tag{7}$$

Pending a more detailed calculation that tracks the cloud's changing internal structure, we simply adopt this expression for all times, and substitute it into equation (6). After utilizing equation (3) as well, we find an expression for the decrease of R with time:

$$\frac{dR}{dt} \;=\; -\frac{3\,\eta}{\sqrt{2}}\sqrt{\frac{G\,M_{\rm cloud}}{R}}\;, \tag{8}$$

which integrates to yield

$$R \;=\; R_\circ\left(1 \;-\; \frac{9\,\eta}{2\,\sqrt{2}}\,\frac{t}{t_\circ}\right)^{2/3}\;. \tag{9}$$

Here, $R_\circ$ is the present ($t = 0$) cloud radius. Equation (8) yields the cloud radius for each past epoch, *i.e.*, for negative values of t. The quantity $t_\circ$ is defined to be

$$t_\circ \equiv \sqrt{\frac{R_\circ^3}{G\,M_{\rm cloud}}} = 7.2\times10^5\,{\rm yr} \tag{10}$$

Equation (8) verifies that the cloud contracts in an accelerating fashion. Indeed, it undergoes a kind of diluted free fall. The time scale for this process, some multiple of the

free fall time $t_\circ$, is set by the (still unknown) parameter η. As the cloud contracts, the speed $V_{\rm turb}$, which is related to R through equation (3), accelerates *upward*. This conclusion is in striking contrast to the current numerical results (see Vázquez-Sendani et al. 2000 for a review), which show the turbulent speed to fall with time. The difference stems from our basic assumption, motivated by the molecular line studies (*e.g.* Myers & Goodman 1988), that the cloud is nearly in virial equilibrium at all times.

5. Discussion

Extending our earlier investigations of other systems, we have documented empirically the acceleration of star formation in the ONC. We have shown that this process occurred at all stellar masses, so that there is no present-day correlation between stellar age and mass. Furthermore, the acceleration was not confined to the cluster's central region, but was global in character. We then surmised, on theoretical grounds, that the parent cloud itself underwent an accelerating contraction, again of a global nature, prior to its recent dispersal.

It is tempting, of course, to relate these two phenomena. Somehow, the contraction of the ONC parent cloud must have stimulated the formation of individual dense cores. This picture is self-consistent only if the dense cores themselves quickly collapsed to stars. Such rapid evolution is at odds with the traditional view that dense cores evolve over a time of order 10^7 yr through ambipolar diffusion (Shu et al. 1987). One intriguing possibility is that ambipolar diffusion itself is enhanced by cloud turbulence (Nakamura & Li 2005).

If star formation generally accelerates, then most molecular clouds should exhibit relatively low rates of starbirth. Where are these quiescent objects? Recall that most stars form within OB associations. The associations themselves are produced by cloud clumps within giant complexes, like the parent entity of the ONC. We suppose that these clumps evolve with time, gaining mass from their surroundings until they undergo accelerating contraction. Only the most massive clumps produce luminous clusters, as was found in the careful study of the Rosette complex by Williams et al. (1995). But if the picture advocated here is correct, then sensitive infrared surveys should reveal lower levels of star formation activity in the remainder of the clump population.

We have stressed that the Trapezium stars are truly anomalous in mass. More specifically, Figure 4 shows that, for objects below about $3\,M_\odot$, the ONC population is spatially homogeneous, but that its central region contains an unusual number of more massive objects. This central concentration could not have been the result of dynamical relaxation in the brief interval since the dispersal of the parent cloud (Bonnell & Davies 1998). These

facts argue for an alternative formation mechanism for massive stars.

Both Bonnell *et al.* (1998) and Stahler et al (2000) have advocated coalescence models. The first authors pictured the merging units to be bare stars and their disks, while the second group invoked dense cores already containing young stars, which subsequently merge. Within the context of a globally contracting cloud, we see how such cores, squeezed by the ambient pressure to sizes smaller than the canonical 0.1 pc, would first coalesce in the central region. Theoretical modeling of this phenomenon would be a welcome contribution.

Finally, our study bears on the eventual fate of the ONC and similar groups. We have found that under 10 percent of the parent cloud mass consisted of stars, just prior to gas dispersal. Including obscured sources within OMC-1 raises this figure. Even with this addition, the fraction is low enough that the stars themselves cannot be bound solely by their mutual gravity. They will disperse into space, forming a typically distended OB association.

It has long been noted that many distant associations appear to contain tight stellar clusters at their centers (see, e.g., Garmany & Stencel 1992). If the ONC is typical in terms of star formation efficiency, then these groups will similarly disperse. In contrast to this view, a number of theorists have proposed that bound clusters originate at the centers of OB associations (Adams 2000; Kroupa et al. 2001). However, their calculations assume that a large fraction (e.g., one third) of a clump's mass is converted to stars before dispersal. In the traditional virial theorem analysis, the fraction necessary to produce a bound system is one half (Hills 1980). Our analysis of the ONC, the nearest rich cluster, indicates that these are overestimates. The origin of bound clusters must lie elsewhere.

In a future study, we plan to follow in more detail the evolution of a cluster-forming cloud. We will track theoretically both the early growth of such entities within a giant complex, as well as the structural changes that accompany their final, accelerating contraction. We also hope to connect quantitatively the rate of star formation at any epoch with the corresponding cloud evolution. Such a calculation would be an important first step toward understanding the larger issue of star formation efficiency on galactic scales.

This project has been aided by illuminating discussions with James Graham, Alessandro Navarrini, and Jon Swift. S. S. was partially supported by NSF Grant AST-9987266.

A. Heat Equation for an Isothermal Cloud

Consider a mass element within a contracting, isothermal cloud of temperature T. The Lagrangian changes in specific entropy, thermal energy, and mass density are related by

$$T\,\Delta s \;=\; \Delta\epsilon_{\rm therm} \;-\; \frac{P}{\rho^2}\,\Delta\rho \tag{A1}$$

When we integrate over all such mass elements, the lefthand side of this equation becomes

$$T\Delta S = -L\Delta t \tag{A2}$$

where S is now the total entropy, and where the luminosity L is assumed to arise from optically thin radiation. If we further invoke mass continuity, in the form

$$\frac{\Delta\rho}{\rho} \;= -\,(\boldsymbol{\nabla}\cdot\mathbf{v})\,\Delta t \tag{A3}$$

then we find

$$-L\,\Delta t \;=\; \Delta E_{therm} + \Delta t \int \frac{dm}{\rho} P\,(\boldsymbol{\nabla}\cdot\mathbf{v}) \tag{A4}$$

where $E_{\rm therm}$ is the total thermal energy.

We recognize dm/ρ as the volume element $d^3\mathbf{x}$. If we do an integration by parts and evaluate the surface term, then the second righthand term in equation (A4) becomes

$$P_\circ\,\Delta V - \Delta t \int d^3\mathbf{x}\,(\mathbf{v}\cdot\boldsymbol{\nabla}P) \tag{A5}$$

where ΔV is the total change in cloud volume. For the pressure gradient $\boldsymbol{\nabla}P$, we employ Euler's equation

$$\boldsymbol{\nabla}P = -\rho\,\boldsymbol{\nabla}\Phi_{\rm grav} - \rho D\mathbf{v}/Dt \tag{A6}$$

where $\Phi_{\rm grav}$ is the gravitational potential. Further manipulation transforms equation (A4) into

$$-L\Delta t = \Delta E_{\rm therm} + P_\circ\Delta V + \Delta K \;+\; \Delta t \int d^3\mathbf{x}\;(\mathbf{v}\cdot\rho\,\boldsymbol{\nabla}\Phi_{\rm grav}) \tag{A7}$$

Here, ΔK is the change in the bulk kinetic energy:

$$K \equiv \int dm\,\frac{v^2}{2} \tag{A8}$$

Since we are not considering a rotating or pulsating cloud, we will henceforth set K equal to zero.

The remaining volume integral appearing in equation (A6) equals the change in $E_{\rm grav}$, the gravitational potential energy. (See Tassoul 1979, p. 147, eq. (127), but note his sign error.) We thus find

$$-L\Delta t = \;\Delta E_{\rm therm} + \Delta E_{\rm grav} + \Delta(P_\circ V) \tag{A9}$$

Dividing by Δt yields the desired heat equation:

$$L = -\frac{dH}{dt} \tag{A10}$$

where the generalized enthalpy $H \equiv E_{\rm therm} + E_{\rm grav} + P_\circ V$. Note, finally, that for a monatomic gas, $E_{\rm therm} = (3/2)\, M_{\rm cloud}\, a_T^2$, where a_T is the isothermal sound speed. When evaluating $E_{\rm therm}$ for the singular isothermal sphere, we have employed this relation, identifying a_T with the turbulent velocity $V_{\rm turb}$.

REFERENCES

Adams, F. C. 2000, ApJ, 542, 964.

Ali, B. & Depoy, D. L. 1995, AJ, 109, 709.

Blitz, L. 1993, in *Protostars and Planets III*, ed. E. H. Levy & J. I. Lunine, (Tucson: U. of Arizona Press), p. 125.

Bonnell, I. A., Bate, M. R., & Zinnecker, H. 1998, MNRAS, 298, 93.

Bonnell, I. A., & Davies M. B. 1998 MNRAS, 295, 691.

Evans, M., Hastings, N., & Peacock, B. 2000 *Statistical Distributions, 3rd ed.* (New York: Wiley).

Garmany, C. D. & Stencel, R. E. 1992, AAS, 94, 211.

Genzel, R. & Stutzki, J. 1989, ARAA, 27, 41.

Goldstein, M. L. 1978, ApJ, 219, 700.

Gordon, M. A. & Churchwell, E. 1970, å, 9, 307.

Hillenbrand, L. A. 1997, AJ, 113, 1733.

Hillenbrand, L. A. & Carpenter, J. M. 2000, ApJ, 540, 236.

Jones, B. F. & Walker, M. F. 1988, AJ, 95, 1755.

Kroupa, P., Aarseth, & Hurley, J. 2001, MNRAS, 321, 699.

Lada, C. J. & Lada. E. A. 2003, ARA&A, 41, 57.

Larson, R. B. 1981 MNRAS, 194, 809.

Mac Low, M.-M. 1999 ApJ, 524, 169.

Miller, G. E. & Scalo, J. M. 1978, PASP, 90, 506.

Myers, P. C. & Goodman, A. A. 1988 ApJ, 326, 27.

Nakamura, F. & Li, Z.-Y. 2005, ApJ, 631, 411.

O'Dell, C. R. 1994, ApJS, 216, 267.

O'Dell, C. R., Walter, D. K., & Dufour, R. J. 1996, ApJ, 399, L67.

Palla, F. & Stahler, S. W. 1999, ApJ, 525, 772 (Paper I).

Palla, F. & Stahler, S. W. 2000, ApJ, 540, 255 (Paper II).

Palla, F. & Stahler, S. W. 2001, ApJ, 553, 299.

Pogge, R. W., Owen, J. M., & Atwood, B. 1992, ApJ, 399, 147.

Prosser, C. F., Stauffer, J. R., Hartmann, L., Soderblom, D. R., Jones, B. F., Werner, M. W., & McCaughrean, M. J. 1994, ApJ, 421, 517.

Roberts, M. S. 1957, PASP, 69,59.

Scalo, J. 1998, in *The Stellar Initial Mass Function*, ed. G. Gilmore, I Parry, & S. Ryan (Cambridge University Press), p. 32.

Shu, F. H., Adams, F. C., & Lizano, S. 1987, ARAA, 25, 23.

Stahler, S. W., Palla, F., & Ho, P. T. P. 2000, in *Protostars and Planets IV*, ed. V. Mannings, A. P. Boss, & S. S. Russell, (Tucson: U. of Arizona Press), p. 327.

Stone, J. M., Ostriker, E. L., & Gammie, C. F. 1998, ApJ, 508, L99.

Tassoul, J.-L. 1979 *Theory of Rotating Stars*, (Princeton: Princeton U. Press), Chapter 6.

Vazquez-Semedani, E., Ostriker, E. C., Passot, T., Gammie, C. F. & Stone, J. M. 2000, in *Protostars and Planets IV*, ed. V. Mannings, A. P. Boss, & S. S. Russell, (Tucson: U. of Arizona Press) p. 3.

Wen, Z. & O'Dell, C. R. 1995, ApJ, 438, 784.

Williams, J. P., Blitz, L. & Stark, A. A. 1995, ApJ, 451, 252.

Zuckerman, B. 1973, ApJ, 183, 863.